IAI Journals.ASM.org

RNA Interference-Mediated Silencing of *Atp6i* Prevents Both Periapical Bone Erosion and Inflammation in the Mouse Model of Endodontic Disease

Junqing Ma,[a,b] Wei Chen,[a] Lijie Zhang,[c] Byron Tucker,[a,d] Guochun Zhu,[a] Hajime Sasaki,[c] Liang Hao,[a] Lin Wang,[b] Hongliang Ci,[a] Hongbing Jiang,[a,b] Philip Stashenko,[c] Yi-Ping Li[a]

Department of Pathology, University of Alabama at Birmingham, Birmingham, Alabama, USA[a]; Institute of Stomatology, Nanjing Medical University, Nanjing, People's Republic of China[b]; Department of Immunology and Infectious Disease, The Forsyth Institute, Cambridge, Massachusetts, USA[c]; Department of Restorative Dentistry in Endodontics, Harvard School of Dental Medicine, Owings Mills, Maryland, USA[d]

Dental caries is one of the most prevalent infectious diseases in the United States, affecting approximately 80% of children and the majority of adults. Dental caries may lead to endodontic disease, where the bacterial infection progresses to the root canal system of the tooth, leading to periapical inflammation, bone erosion, severe pain, and tooth loss. Periapical inflammation may also exacerbate inflammation in other parts of the body. Although conventional clinical therapies for this disease are successful in approximately 80% of cases, there is still an urgent need for increased efficacy of treatment. In this study, we applied a novel gene-therapeutic approach using recombinant adeno-associated virus (AAV)-mediated Atp6i RNA interference (RNAi) knockdown of *Atp6i/TIRC7* gene expression to simultaneously target periapical bone resorption and periapical inflammation. We found that *Atp6i* inhibition impaired osteoclast function *in vitro* and *in vivo* and decreased the number of T cells in the periapical lesion. Notably, AAV-mediated *Atp6i/TIRC7* knockdown gene therapy reduced bacterial infection-stimulated bone resorption by 80% in the mouse model of endodontic disease. Importantly, *Atp6i*$^{+/-}$ mice with haploinsufficiency of *Atp6i* exhibited protection similar to that in mice with bacterial infection-stimulated bone erosion and periapical inflammation, which confirms the potential therapeutic effect of AAV-small hairpin RNA (shRNA)-*Atp6i/TIRC7*. Our results demonstrate that AAV-mediated *Atp6i/TIRC7* knockdown in periapical tissues can inhibit endodontic disease development, bone resorption, and inflammation, indicating for the first time that this potential gene therapy may significantly improve the health of those who suffer from endodontic disease.

The World Health Organization estimates that between 60% and 90% of schoolchildren and the vast majority of adults in industrialized countries suffer from dental caries and its symptoms, with rates in developing countries being even higher (1). Dental caries, which is one of the most common oral diseases, is caused by infections with *Streptococcus mutans* and other acidogenic bacteria that result in demineralization of tooth enamel. Following this, the infection may invade the pulpal tissues of the tooth. The progression of this microbial infection extends to the root of the tooth and leads to periapical bone resorption surrounding the periodontal ligament (PDL) space (2–4). Currently, endodontic disease is treated by mechanical removal of the infected pulp tissue, followed by obturation of the root canal space with an inert filling material such as gutta percha. If successful, regeneration of the resorbed periapical bone occurs, but it may take as long as 2 years, and in some cases complete healing is never achieved. Therefore, an adjunctive therapy that could reduce the initial damage and accelerate the healing process would be extremely beneficial.

Osteoclasts are the primary cells that mediate bone resorption, including in endodontic disease (2, 5). Osteoclasts function to remove the mineral components of bone by extracellular acidification, following which bone matrix proteins are degraded by proteases, including cathepsin K. Osteoclasts decrease the pH at the cell-to-bone interface via a multiunit vacuolar proton pump apparatus. In our previous investigations, we demonstrated that *Atp6i*, which encodes a subunit of the osteoclast proton pump, is critical for the extracellular acidification that is necessary for osteoclast-mediated bone resorption (6, 7). Atp6i knockout mice have profound osteopetrosis and lack tooth eruption; hence, this gene is an attractive target for inhibiting osteoclast function (7). In addition, *Atp6i* has been shown to be expressed specifically in osteoclasts (6, 7).

It has also been established that the receptor activator of nuclear factor κβ ligand (RANKL), which stimulates osteoclast differentiation, is expressed by human dental pulp cells (8–10), as well as by activated T cells, which are induced by pulpal infection. This pathway is critical for osteoclastogenesis and osteoclast activation in chronic inflammatory disease processes such as periodontitis (11, 12). Of interest, an isotype of *Atp6i*, *TIRC7*, is expressed specifically in T cells as a transmembrane protein that is upregulated during T-cell activation (13). The function of *TIRC7*

Received 20 July 2012 **Returned for modification** 3 September 2012
Accepted 6 November 2012
Published ahead of print 19 November 2012
Editor: A. J. Bäumler
Address correspondence to Yi-Ping Li, ypli@uab.edu, or Wei Chen, wechen@uab.edu.
J.M. and W.C. contributed equally to this work.
Supplemental material for this article may be found at http://dx.doi.org/10.1128/IAI.00756-12.

doi:10.1128/IAI.00756-12

was examined *in vitro* and *in vivo* via *TIRC7*$^{-/-}$ mouse models, and the results indicated that *TIRC7* exerts significant regulation of T- and B-cell activation (14). In addition, studies have demonstrated increased survival of organ allograft transplants with anti-*TIRC7* monoclonal antibody therapy (15).

The gene transcript for *Atp6i* and *TIRC7* is located on chromosome 11q13 and is alternatively spliced depending on the cell type (T cells or osteoclasts) in which the gene is expressed. Although there are 1,939 bp shared by the *Atp6i* and *TIRC7* transcripts in T and B cells and osteoclasts (13), there are 518 unique base pairs in the exon for the *TIRC7* transcript in T and B cells and 690 unique base pairs in the *Atp6i* transcript in osteoclasts (13). These shared and unique sequences of the *Atp6i* gene provide possible regions for the design of a short hairpin RNA (shRNA) that can be used for viral vector-mediated *Atp6i* RNA interference (RNAi) knockdown for dual silencing of *Atp6i* in osteoclasts and *TIRC7* in T cells.

Adeno-associated virus (AAV) silencing is a novel and effective tool that has been proven safe and well tolerated in humans in a clinical setting, suggesting that *in vivo* gene therapy is safe and that it causes only a very mild immune response (16, 17). Furthermore, studies have recently demonstrated AAV's impressive ability to be effective long-term at various doses (18). AAV is capable of inserting a specific therapeutic gene with high certainty into the genome, of maintaining long-term gene expression, and of being nonpathogenic. Recently, it has even exhibited successful local knockdown, allowing gene therapy with localized and specific manipulation of the expression of single or multiple genes *in vivo* (19). Lentivirus illustrated successful gene transfer in our previous investigation (6). In addition, it is of great interest to compare the gene transfer capability of lentivirus to that of other viral systems to establish literature for support of as efficient or more efficient and safer viral alternatives for gene therapy. Therefore, we use the AAV/RNAi knockdown system to investigate the effect of *Atp6i* silencing, due to its unique attributes, and compare the therapeutic value of AAV to that of lentivirus.

The aim of the present investigation was to rigorously determine the therapeutic potential of simultaneous knockdown of *Atp6i* and *TIRC7* in the prevention of polymicrobially induced periapical bone loss in the mouse model through the use of locally delivered AAV-*Atp6i* RNAi, which resulted in silencing of both *Atp6i* and its isoform, *TIRC7*. In addition, this study sought to determine if AAV is a viable alternative for successful RNAi gene delivery. This is the first study to investigate the use of AAV-mediated knockdown of *Atp6i* as a potential target for gene therapy to treat endodontic disease.

MATERIALS AND METHODS

Animals. Seven- to 8-week-old male wild-type (WT) BALB/cJ mice were purchased from the Jackson Laboratory, Bar Harbor, ME. *Atp6i*$^{+/-}$ mice previously generated by our lab (7) were backcrossed for 4 generations from the C57BL/6J onto the BALB/cJ background. The animals were maintained in the University of Alabama at Birmingham animal facility and were given laboratory chow and distilled water *ad libitum*. All experimental protocols were approved by the NIH and the Institutional Animal Care and Use Committee of the University of Alabama at Birmingham (animal protocol number 11090909236) (20, 21).

Cells and cell culture. Preosteoclasts and mature osteoclasts in primary culture were generated from mouse bone marrow (MBM) as described previously (6, 22, 23). Briefly, MBM was obtained from tibiae and femora from female WT BALB/cJ mice and *Atp6i*$^{+/-}$ mice as described previously (24, 25). MBM (1×10^5 to 2×10^5) were seeded into the wells of 24-well plates; 1×10^6 MBM were seeded into wells of 6-well plate. MBM were cultured in alpha-modified Eagle's medium (α-MEM; GIBCO-BRL) with 10% fetal bovine serum (FBS; GIBCO-BRL) containing 10 ng/ml macrophage colony-stimulating factor (M-CSF) (R&D Systems, Minneapolis, MN). After 24 h, cells were cultured further in the presence of 10 ng/ml RANKL (R&D Systems) and 10 ng/ml M-CSF for an additional 96 h to generate mature osteoclasts.

Design and construction of shRNA. Using the Dharmacon siDESIGN Centre as described in our recent publication (6), we generated an shRNA that would simultaneously target exon 15 of *Atp6i* and exon 10 of *TIRC7*. As a control vector, we used AAV-H1-shRNA-Luc-YFP (gift from Sonoko Ogawa), which contains a luciferase (Luc)-specific shRNA and a yellow fluorescent protein (YFP) cassette (26). AAV-H1 contains a human polymerase III (PolIII) H1 promoter for expression of shRNA, as well as an independent enhanced green fluorescent protein (EGFP) expression cassette (19). The H1 promoter shRNA expression cassette was cloned into the AAV construct as described previously (19, 27, 28). The following shRNA oligonucleotides were annealed and cloned downstream of the H1 promoter of AAV-H1 into BglII and HindIII sites to produce AAV-H1-shRNA-*Atp6i/TIRC7*: 5′-GATCCCCGTATCCTCATTCACTTCAT **TTCAAGAGA**ATGAAGTGAATGAGGATACTTTTTGGAAA-3′. Nucleotides specific for targeting *Atp6i/TIRC7* are underlined. The bold type signifies the 9-bp hairpin spacer.

AAV RNAi viral production and purification. An AAV helper-free system was purchased from Stratagene. Viral production was accomplished using a triple-transfection, helper-free method, and viruses were purified with a modified version of a published protocol (27). Briefly, HEK 293 cells were cultured in ten 150- by 25-mm cell culture dishes and transfected with pAAV-shRNA, pHelper, and pAAV-RC plasmids (Stratagene) using a standard calcium phosphate method. Cells were collected after 60 to 72 h and lysed by shaking with chloroform at 37°C for 1 h. Sodium chloride was then added and shaken at room temperature for 30 min. The stock was spun at 12,000 rpm for 15 min, and the supernatant was collected and cooled on ice for 1 h with polyethylene glycol 8000 (PEG 8000). The solution was spun at 11,000 rpm for 15 min, and the pellet was treated with DNase and RNase. After addition of chloroform and a 5-min centrifugation at 12,000 rpm, the number of purified virus particles in the aqueous phase was 1×10^{10}/ml. The AAV particle titer was determined using an AAV quantitation titer kit (Cell Biolabs, Inc.). To confirm the effect of silencing, we examined the expression of *Atp6i* in osteoclasts using qPCR, Western blotting, and immunofluorescence.

Pulp exposure, bacterial infection, and transduction of AAV vectors. Pulp exposure was performed as described previously (3, 29). In brief, mice were anesthetized by an intraperitoneal injection of 62.5 mg/kg ketamine and 12.5 mg/kg xylazine. The dental pulps of the mandibular first molars were exposed with a 1/4 round carbide bur powered by a variable-speed electric rotary hand piece (Osada Electric, Los Angeles, CA) under a surgical microscope (model MC-M92; Seiler, St. Louis, MO); the exposure was approximately 1.5 to 2.0 mm in diameter. Stainless steel hand files (number 8; Dentsply Maillefer, Johnson City, TN) and stainless steel rotary files (number 15; Dentsply Maillefer) were used to establish canal patency.

Bacterial culture and infection protocols were conducted as described previously (30). In brief, exposed pulps were infected with a mixture of four common human endodontic pathogens, including *Prevotella intermedia* ATCC 25611 (American Type Culture Collection, Manassas, VA), *Fusobacterium nucleatum* ATCC 25586, *Peptostreptococcus micros* ATCC 33270, and *Streptococcus intermedius* ATCC 27335. All four species were cultured under strictly anaerobic conditions (80% N_2, 10% H_2, and 10% CO_2) in broth for 7 to 8 days. Microbes were harvested and resuspended, and cell concentrations of each species were determined via optical density readings at 600 nm (OD_{600}; 1 OD unit equals 6.67×10^8 bacteria). The cell density of each species was adjusted to 10^{10} per ml and mixed in phosphate-buffered saline (PBS) containing 3% methylcellulose. Ten mi-

croliters of the polymicrobial solution was inoculated into the access opening of each molar and carried to the periapical tissues using a number 8 endodontic file. Exposed pulps were left open to the oral environment for 24 h.

Transduction was carried out by injecting the viral vectors into the periapical tissues as described elsewhere, with modifications (19). Briefly, on day 1 and day 3 after pulpal infection, mice were anesthetized, and approximately 3 μl (2×10^9 packaged particles in PBS) of either AAV-shRNA-*Atp6i/TIRC7*, referred to here as AAV-sh-*Atp6i* ($n = 21$), or AAV-sh-Luc-YFP ($n = 21$) was injected through the tooth root into the apical periodontium. Mice ($n = 21$) without pulp exposure and infection served as negative controls (normal controls). As positive controls (diseased controls), mice ($n = 21$) were subjected to pulp exposure and infection but were not treated with either of the viral vectors. All exposure sites were sealed with self-curing composite resin after AAV transduction. Eradication of infected microorganisms was not completed in this therapy.

Harvest and preparation of samples. Most animals were sacrificed by CO_2 inhalation on day 42 after infection for sample collection, except that some mice were sacrificed on day 21 or day 28. The mandibles were removed and hemisected. After removal of soft tissue, the left hemimandibles were fixed in 4% formaldehyde for 24 h and stored in 70% ethanol until micro-computed tomography (micro-CT) analysis of bone loss. The right hemimandibles were fixed in 4% paraformaldehyde and prepared for histological analysis. In brief, samples were fixed in 4% formaldehyde for 24 h, washed with PBS, decalcified in 10% EDTA for 10 days (EDTA was replenished each day), transferred to 30% sucrose for 24 h, embedded in frozen section compound (FSC 22; Surgipath, Leica Microsystems), and stored at −80°C prior to cryostat sectioning. For total RNA and cytokine enzyme-linked immunosorbent assays (ELISAs), the periapical tissues surrounding the mesial and distal roots were extracted from the mandible together with surrounding bone in a block specimen using a surgical microscope. For RNA extraction, periapical tissues were rinsed in prechilled PBS, weighed (3 to 5 mg/tissue), and immediately placed in RNAlater-ICE (Invitrogen) overnight at 4°C and stored at −80°C until RNA extraction. For ELISAs, the periapical tissues were rinsed in cold PBS, weighed (3 to 5 mg/tissue), and immediately frozen at −80°C until protein extraction.

Micro-computed tomography (micro-CT) analysis. Micro-computed tomography (micro-CT) scans were evaluated for bone loss as described previously (31). In brief, the most centrally located section that provided a cross-sectional view of the crown and distal root of the mandibular first molar and that exhibited a patent root canal apex was selected for quantification of periapical bone loss. The cross-sectional area of the periapical lesions was selected via Adobe Photoshop (Adobe Systems, San Jose, CA) and measured with ImageJ software (National Institutes of Health, Bethesda, MD). Bone loss was also evaluated by three-dimensional micro-CT analyses as described previously (32, 33). Briefly, the picture that showed the largest target root canal was selected as the baseline image. For each sample, approximately 10 microtomographic slices with an increment of 12 μm were acquired in front of and behind the baseline image. From the three-dimensional stack of micro-CT images, a "pivot" section was the periapical area of the tooth.

Histological analysis. Samples were fixed in 4% paraformaldehyde for 24 h, decalcified in 10% EDTA for 10 days, and embedded in paraffin or processed as frozen sections. To detect osteoclasts, TRAP (tartrate-resistant acid phosphatase) staining was performed by standard methods.

Western blotting. Western blot analysis of Atp6i expression in MBM stimulated with M-CSF/RANKL for 3 days and transduced with AAV-sh-Luc-YFP or AAV-sh-*Atp6i* was performed as described using rabbit anti-Atp6i antibody previously generated in our lab (7, 22, 34). Immunoblots were visualized and quantified using a Fluor-S Multi-Imager and Multi-Analyst software (Bio-Rad). Western blot analysis of Atp6i expression in MBM obtained from *Atp6i*$^{+/-}$ mice and *Atp6i*$^{+/+}$ mice was performed similarly. The expression of tubulin or actin served as a control.

TABLE 1 TaqMan-based qPCR primers and probes

Gene	Applied Biosystems assay ID[a]
Acp5	Mm00475698_m1
Tcirg1 (*Atp6i*)	Mm00469394_m1
Calcr	Mm00432271_m1
Csf1r (CD115)	Mm01266652_m1
Ctsk	Mm00484039_m1
Tnfsf11 (RANKL)	Mm00441906_m1
IL-6	Mm00446190_m1
*IL-1*α	Mm00439620_m1
*IL-1*β	Mm01336189_m1
*IL-17*α	Mm00439618_m1

[a] Identification number for each primer/probe set.

Immunofluorescence analysis. Immunofluorescence analysis was performed as previously described (7), using anti-Atp6i (7) and rabbit polyclonal anti-CD3 (Abcam, Cambridge, MA) as the primary antibodies. Observations were performed by detecting epifluorescence using a Zeiss Axioplan microscope. Nuclei were visualized with 1 μg/ml DAPI (4′,6-diamidino-2-phenylindole; Sigma). The experiments were performed in triplicate on three independent occasions.

Immunohistochemistry analysis. We performed immunohistochemistry using corresponding sections of mandibles from uninfected mice or infected mice treated with AAV-sh-Luc-YFP or with AAV-sh-*Atp6i*. Slides were analyzed by immunohistochemistry for expression and localization of proteins using the macrophage marker F4/80 (rat monoclonal, 1:200) (eBioscience, San Diego, CA). Vector stain ABC kit anti-rat IgG peroxidase polymer detection systems, along with a diaminobenzidine (DAB) kit (Vector Laboratories, Burlingame, CA) as a substrate, were used for the peroxidase-mediated reaction. The experiments were performed in triplicate on three independent occasions.

Acridine orange staining. Acid production was determined using acridine orange as described previously (7). Osteoclasts transduced with viral vectors after 48 h of RANKL/M-CSF stimulation were incubated in α-MEM containing 5 μg/ml of acridine orange (Sigma) for 15 min at 37°C and chased for 10 min in fresh medium without acridine orange. The cells were observed under a fluorescence microscope with a 490-nm excitation and a 525-nm arrest filter. The experiment was performed in duplicate on four independent occasions.

***In vitro* bone resorption assays.** Bone resorption activity was assessed as described previously (35), with modifications. MBM were cultured on bovine cortical bone slices in 24-well plates and were transduced with viral vectors after 48 h of RANKL/M-CSF stimulation. Bone slices were harvested after 6 days, and culture medium was collected. The cells on bone slices were subsequently removed with 0.25 M ammonium hydroxide and mechanical agitation. Bone slices were subjected to scanning electron microscopy (SEM) using a Philips 515 SEM. We also assessed *in vitro* bone resorption using wheat germ agglutinin (WGA) to stain exposed bone matrix proteins. The assays were performed in triplicate. The data were quantified by measuring the percentage of the areas resorbed in three random resorption sites, as determined using ImageJ analysis software obtained from the National Institutes of Health (NIH).

RNA extraction and real-time quantitative PCR (qPCR). For RNA extraction, periapical tissue samples were transferred to tubes filled with beads (Nextadvance Company) and homogenized using a blender (Bullet Blender, Nextadvance Company). RNA was extracted in TRIzol reagent (Invitrogen). The extracted RNA was reverse transcribed using a VILO master kit (Invitrogen). Real-time quantitative PCR (qPCR) was performed as described previously (36, 37) using TaqMan probes purchased from Applied Biosystems (Table 1). Briefly, cDNA fragments were amplified by TaqMan fast advanced master mix (Applied Biosystems). Fluorescence from each TaqMan probe was detected by a StepOne real-time PCR system (Applied Biosystems, Foster City). The mRNA expression level of the housekeeping gene *Hprt*, encoding hy-

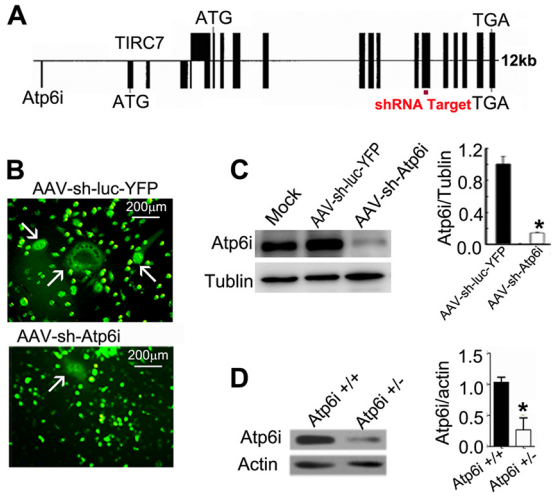

FIG 1 AAV-sh-*Atp6i* simultaneously targets *Atp6i* and *TIRC7* mRNA and efficiently knocks down the expression of *Atp6i*. (A) Diagram of loci illustrating *Atp6i* and *TIRC7* zones of homology and shRNA specific for *Atp6i/TIRC7* mRNA. (B) MBM stimulated with M-CSF/RANKL for 3 days and transduced with AAV-sh-Luc-YFP or AAV-sh-*Atp6i*. Fluorescence indicates effective transduction of preosteoclasts and osteoclasts (white arrows). (C) Western blot of *Atp6i* expression in MBM stimulated with M-CSF/RANKL for 3 days and transduced with AAV-sh-Luc-YFP or AAV-sh-*Atp6i* or left untreated (mock). Quantification of Western blot analysis demonstrates that AAV-sh-*Atp6i*-treated osteoclasts have significantly reduced expression of *Atp6i*. (D) Western blot showing that the *Atp6i* expression level was significantly decreased in $Atp6i^{+/-}$ mice osteoclasts compared to $Atp6i^{+/+}$ mice. *, $P < 0.01$.

poxanthine-guanine phosphoribosyl transferase, was used as an endogenous control, and specific mRNA expression levels were calculated as ratios to the level of *Hprt* expression. Experiments were repeated at least three times.

Protein extraction for ELISAs. For protein extraction, the frozen periapical tissue samples from uninfected mice (normal controls) or infected mice treated with AAV-sh-Luc-YFP or with AAV-sh-*Atp6i* were homogenized in 1 ml of lysis buffer. The mixture was incubated at 4°C for 1 h, and the supernatant was collected after centrifugation and stored at −80°C until the assay. Enzyme-linked immunosorbent assays (ELISAs) were carried out as described previously (30, 38) employing commercially available ELISA kits for the following proteins: interleukin 1α (IL-1α; Endogen, Cambridge, MA; sensitivity, 6 pg/ml), IL-6 (BioSource International, Camarillo, CA; 8 pg/ml), and IL-17α. All assays were conducted in accordance with the manufacturer's instructions. Results were expressed as picograms of cytokine/mg tissue.

Statistical analysis and data quantification analysis. Experimental data were reported as means ± standard deviations (SD) of triplicate independent samples. Data were analyzed with the two-tailed Student's *t* test. *P* values of <0.05 were considered significant. To calculate the degree of protection by the AAV vectors, the difference between the bone volume-to-total volume (BV/TV) ratios of the normal group and those of the AAV-sh-Luc-YFP and AAV-sh-Atp6i treatment groups, as determined by micro-CT, were used.

RESULTS

AAV-sh-*Atp6i* simultaneously targeted *Atp6i* and *TIRC7* mRNA and efficiently knocked down the expression of *Atp6i*. To enable simultaneous inhibition of inflammation and bone resorption through a single target, we generated shRNA that would simultaneously target exon 15 of *Atp6i* (which encodes a subunit of the osteoclast-specific proton pump) and exon 10 of *TIRC7* (T-cell immune response cDNA 7, an isoform of ATP6i) (Fig. 1A). AAV.H1 contains a human PolIII H1 promoter for shRNA expression, as well as an independent enhanced green fluorescent protein (EGFP) expression cassette, and has been used to successfully knockdown estrogen receptor α *in vivo* (19). Efficient infection with our AAV-sh-*Atp6i* was achieved using a titer of approximately 6×10^{11} DNase-resistant particles (DRP)/ml, as shown by the high percentage of target cells expressing green fluorescent protein (GFP) (Fig. 1B). To confirm the effect of *Atp6i* silencing, we examined the expression of *Atp6i* in mouse bone marrow (MBM) cells isolated from wild-type BALB/cJ mice, cultured with M-CSF and RANKL to generate osteoclasts, and transduced *in vitro* with AAV-sh-*Atp6i* or AAV-sh-Luc-YFP as a control. Western blot analysis revealed that osteoclasts transduced with AAV-sh-*Atp6i* had an 80% reduction in *Atp6i* expression compared to untreated osteoclasts or osteoclasts transduced with AAV-sh-Luc-YFP (Fig. 1C). To verify if $Atp6i^{+/-}$ mice could serve as an alternative model for knockdown, we performed Western blot analysis and determined that the level of *Atp6i* protein was significantly reduced in $Atp6i^{+/-}$ mice compared to $Atp6i^{+/+}$ mice (Fig. 1D). $Atp6i^{+/-}$ mice were used, since $Atp6i^{-/-}$ mice die within 3 weeks of birth. Overall, our results indicate that AAV-sh-*Atp6i*, which targets *Atp6i* and its isoform *TIRC7*, efficiently reduces *Atp6i* expression.

Depletion of *Atp6i* impaired extracellular acidification by osteoclasts, osteoclast-mediated bone resorption, and osteoclastogenesis. Our previous study with $Atp6i^{-/-}$ mice revealed

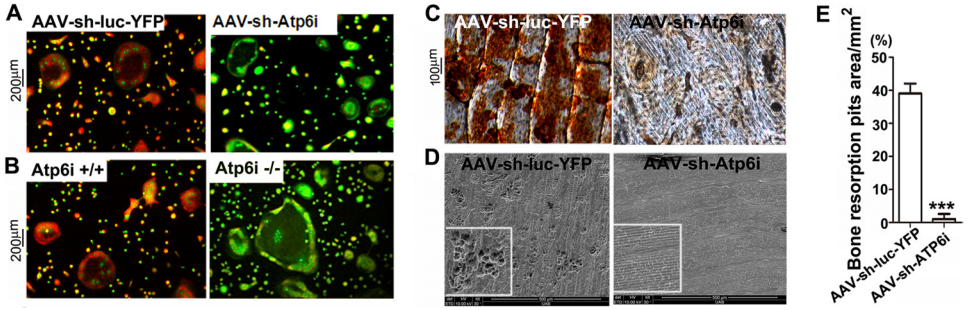

FIG 2 Depletion of *Atp6i* impaired extracellular acidification by osteoclasts and osteoclast-mediated bone resorption. (A and B) Acridine orange staining of osteoclasts, including cells without fusion (<3 nuclei). Both osteoclasts transduced with AAV-sh-*Atp6i* and osteoclasts from $Atp6i^{-/-}$ mice show a lack of extracellular acidification (orange) compared to osteoclasts from the AAV-sh-Luc-YFP treatment group or $Atp6i^{+/+}$ mice. (C and D) Resorption lacunae were visualized by wheat germ agglutinin (WGA) (C) and scanning electron microscopy (SEM) (D). Depletion of *Atp6i* totally blocked osteoclast-mediated bone resorption. (E) Quantification of resorption pits on bone slices. ***, $P < 0.005$.

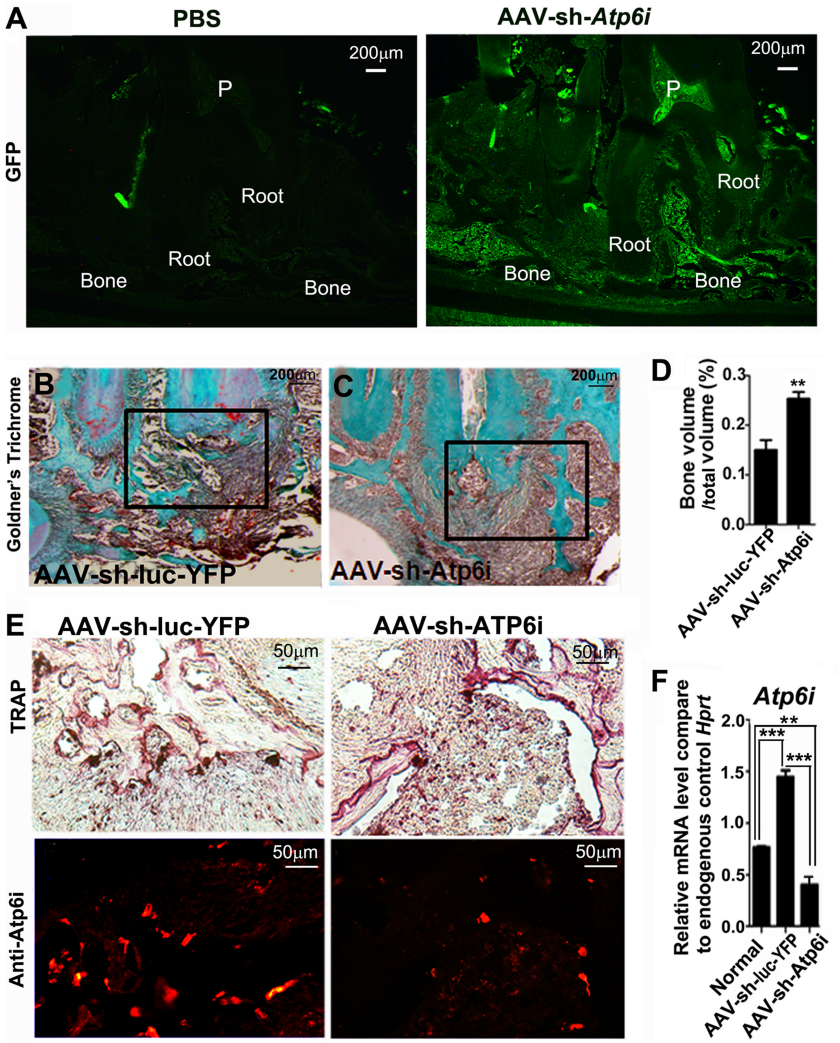

FIG 3 Infection induced periapical inflammation and bone resorption, which is reduced by AAV-sh-*Atp6i* treatment. (A) Fluorescent eGFP expression by AAV-infected cells in groups treated with PBS or AAV-sh-*Atp6i*. (B and C) Goldner's trichrome staining reveals that AAV-sh-*Atp6i* treatment (C), compared to AAV-sh-Luc-YFP treatment (B), protects infected mice from bone resorption in the periapical region. (D) Quantification of the ratio of bone volume (BV) to total volume (TV) of boxed areas in panels B and C. (E) TRAP staining and immunofluorescence staining for Atp6i (red) of sections from infected mice treated with AAV-sh-Luc-YFP or AAV-sh-*Atp6i*. (F) qPCR of *Atp6i* in uninfected mice (normal), infected mice treated with AAV-sh-Luc-YFP, and infected mice treated with AAV-sh-*Atp6i*. *Hprt* was used as an endogenous control. P, pulp. **, $P < 0.01$; ***, $P < 0.005$.

that *Atp6i* is an osteoclast-specific proton pump subunit essential for osteoclast-mediated extracellular acidification in bone resorption (7). We found that osteoclasts transduced with AAV-sh-*Atp6i* and osteoclasts from *Atp6i*$^{-/-}$ mice show a lack of extracellular acidification compared to osteoclasts transduced with AAV-sh-Luc-YFP or osteoclasts from *Atp6i*$^{+/+}$ mice (Fig. 2A and B). Compared to AAV-sh-Luc-YFP treatment, AAV-sh-*Atp6i*-mediated *Atp6i* knockdown greatly reduced osteoclast-mediated bone resorption in bone slices *in vitro* (Fig. 2C), indicating that AAV-sh-*Atp6i* dramatically inhibits bone-resorptive function, as assessed by scanning electron microscopy (SEM) (Fig. 2D and E). These data demonstrate that AAV-sh-*Atp6i* powerfully inhibits extracellular acidification by osteoclasts and osteoclast-mediated bone resorption.

AAV-sh-*Atp6i* treatment reduces infection induced periapical inflammation and bone resorption. Dental pulp infections were induced, and the effect of AAV-sh-Atp6i on inflammatory bone destruction was determined. Local delivery of the AAV vector was monitored by fluorescence analysis, which confirmed the presence of the AAV-sh-*Atp6i* vector in periapical tissues (Fig. 3A). In order to determine the therapeutic effect of AAV-sh-*Atp6i* on periapical bone destruction, we performed Goldner's trichrome staining and found that AAV-sh-*Atp6i* treatment (Fig. 3C) protects infected mice from bone resorption in the periapical region compared to AAV-sh-Luc-YFP treatment (Fig. 3B). The extent of bone destruction was quantified by micro-computed tomography. We found that AAV-sh-Atp6i-treated mice had higher bone volume/total volume (BV/TV) ratios than the AAV-sh-Luc-YFP controls, indicating that AAV-sh-*Atp6i* protects against infection-induced bone resorption (Fig. 3D). We also performed TRAP staining on the AAV-sh-Luc-YFP- and AAV-sh-*Atp6i*-treated groups (Fig. 3E). As expected, there was less expression of *Atp6i* in the AAV-sh-*Atp6i*-treated group than in the AAV-sh-Luc-YFP-treated group. The relative mRNA levels,

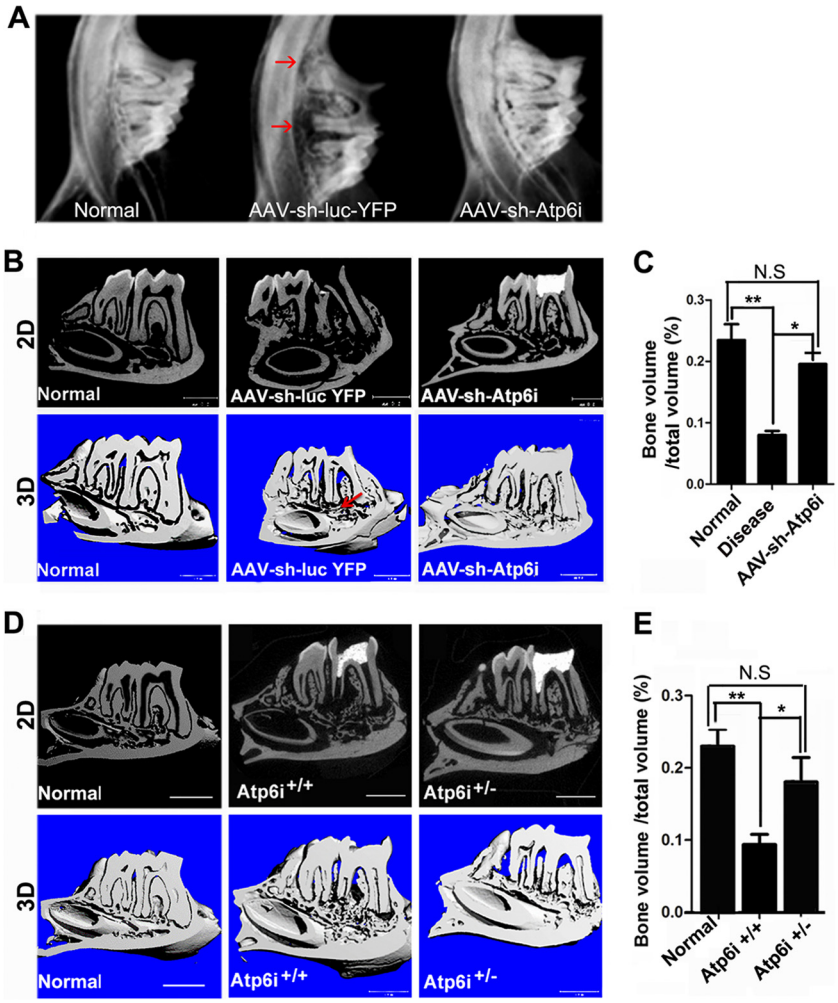

FIG 4 *Atp6i* depletion reduced infection-stimulated periapical bone resorption. (A) X-ray imaging of the crown and distal root of the mandibular first molar and patent apical foramen from WT BALB/cJ mice that did not receive polymicrobial infection or any form of treatment (normal), infected mice treated with AAV-sh-Luc-YFP (negative control), and infected mice treated with AAV-sh-*Atp6i*. (B) Micro-computed tomography (micro-CT) analysis of the mandibular first molar in WT BALB/cJ mice that did not receive polymicrobial infection or any form of treatment (normal), infected mice treated with AAV-sh-Luc-YFP, and infected mice treated with AAV-sh-*Atp6i*. Red arrows indicate severe periapical bone loss. (C) Quantification of the ratio of bone volume to total volume measured for periapical lesions in panel B. (D) Micro-CT analysis of the mandibular first molar in infected $Atp6i^{+/+}$ and $Atp6i^{+/-}$ mice, and uninfected mice (normal). (E) Quantification of the bone volume/total volume ratio for periapical lesions in panel D. *, $P < 0.05$; **, $P < 0.01$. The top rows in panels B and D are typical 2D micro-computed tomography (micro-CT) images, while the bottom rows are 3D reconstitutions. Bar, 1 mm.

using *Hprt* as an endogenous control (Fig. 3F), showed that there were significantly lower mRNA levels in the AAV-sh-*Atp6i* treatment group than in the AAV-sh-Luc-YFP or the uninfected normal group.

***Atp6i* depletion reduced infection-stimulated periapical bone resorption.** In order to determine the efficacy of AAV-shRNA-*Atp6i* in reducing the extent of endodontic disease, we used a model of periapical lesion induction as described previously (30). Exposed dental pulps were infected with a mixture of four common endodontic pathogens: *Prevotella intermedia* (ATCC 25611), *Fusobacterium nucleatum* (ATCC 25586), *Peptostreptococcus micros* (ATCC 33270), and *Streptococcus intermedius* (ATCC 27335). The amount of periapical bone resorption surrounding the distal root of the mandibular first molar was analyzed using X-ray imaging and micro-CT (Fig. 4A and B). The bone resorption in the infected group treated with the control AAV-sh-Luc-YFP was significantly greater than that in the normal group, while AAV-sh-*Atp6i* protected against periapical bone resorption (Fig. 4B). We also performed quantitative analysis of the ratio of bone volume (BV) to total volume (TV) in each group. We found that the AAV-sh-Atp6i treated group had approximately 80% less infection-induced bone loss than the control AAV-sh-Luc-YFP treatment group (Fig. 4c). We also performed a micro-CT analysis of infection-induced bone loss in $Atp6i^{+/+}$ and $Atp6i^{+/-}$ mice (Fig. 4D). Quantitative analysis of BV/TV showed that there was more bone loss in the $Atp6i^{+/+}$ mice, confirming the above results with AAV knockdown (Fig. 4E).

AAV-mediated Atp6i knockdown decreased the number of inflammatory cells in periapical lesions. In order to determine the effect of AAV-mediated *Atp6i* knockdown on the number of T cells in periapical lesions, we performed hematoxylin and eosin (H&E) staining of periapical root sections from uninfected mice (Fig. 5A), or infected mice treated with AAV-sh-Luc-YFP (Fig. 5B) or AAV-sh-*Atp6i* (Fig. 5C). The results showed fewer mono-

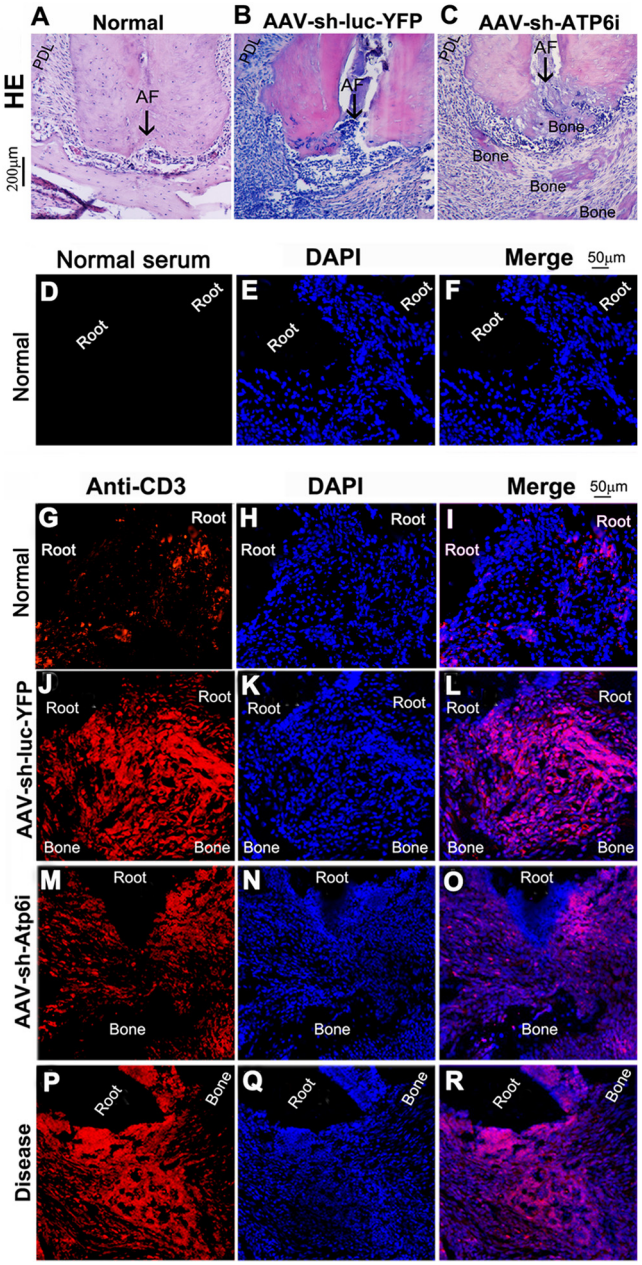

FIG 5 AAV-mediated *Atp6i* knockdown decreased the number of T cells in periapical lesions. (A to C) H&E staining of the periapical root sections from uninfected mice (normal) (A) or infected mice treated with AAV-sh-Luc-YFP (B) and AAV-sh-*Atp6i* (C). (D to R) Immunofluorescence staining of CD3-positive (red) T cells in periapical lesions in uninfected mice (normal) (G to I), infected mice treated with AAV-sh-Luc-YFP (J to L) or AAV-sh-*Atp6i* (M to O), or untreated infected mice (disease control) (P to R). Nuclei were labeled using the DNA stain DAPI (blue). (D to F) Negative control group (without primary antibody). AF, apical foramen; PDL, periodontal ligament.

nuclear leukocytes in the AAV-sh-*Atp6i* treatment group (Fig. 5C), as indicated by the dark staining nuclei. We also performed immunofluorescence staining of CD3 positive T cells in uninfected mice (Fig. 5g,h) in infected mice that were treated with AAV-sh-Luc-YFP (Fig. 5J and K) or AAV-sh-*Atp6i* (Fig. 5M and N), as well as in untreated disease controls (Fig. 5P and Q). Normal serum was used without the primary antibody to provide a negative-control group (Fig. 5D and E). We then merged each set of images for comparison (Fig. 5F, I, L, O, and R). These images indicate fewer visible nuclei in the AAV-sh-*Atp6i* group than in the AAV-sh-Luc-YFP group. AAV-sh-*Atp6i* knockdown thus also decreased the number of T cells in periapical lesions.

AAV-sh-*Atp6i* reduced the expression of osteoclast marker genes and cytokines in the periapical lesion to closer-to-normal expression levels. To evaluate the effect of *Atp6i* silencing on the levels of interleukin-1α (IL-1α) and other regulatory cytokines in inflammatory periapical tissues, qPCR and ELISA of extracted periapical tissues were used. The relative mRNA expression levels showed that osteoclast marker genes, including those encoding cathepsin K and acid phosphatase 5 (*Acp5*), were increased in the AAV-sh-Luc-YFP treatment group compared to the AAV-sh-*Atp6i* group. The macrophage marker CD115 (Mcsfr) was reduced by AAV-sh-*Atp6i*. *Atp6i* knockdown also reduced the expression of IL-6, which is important for osteoclast differentiation (Fig. 6A). The IL-1α and IL-17α levels were increased in the infected mice and were decreased by AAV-sh-*Atp6i* treatment (Fig. 6b).

DISCUSSION

Endodontic therapy is used in the clinical setting to remove necrotic infected pulp tissue and inhibit the local inflammatory reaction in the periapical region. Complete healing of bone even after successful treatment may take up to 2 years; hence, reducing the severity of disease would be important for the more rapid recovery of homeostasis. In this study, we tested a novel gene therapy using AAV2 as a vector to knock down the target gene *Atp6i*, whose product plays dual roles in endodontic disease, to simultaneously reduce bone resorption and inflammation. Atp6i is a subunit of the osteoclast-specific proton pump (7) and TIRC7 is a T-cell immune response isoform of Atp6i (14). This study investigated a novel approach for treatment through simultaneous adeno-associated virus (AAV) knockdown of *Atp6i* and *TIRC7*. Since patients with periodontal or endodontic disease suffer from both inflammation-induced tissue damage and bone loss, a single target that can target both manifestations may be ideal for reducing disease severity. Our AAV vector targeted exon 15 of *Atp6i* and exon10 of *TIRC7* (Fig. 1) and efficiently knocked down *Atp6i in vitro*. The knockdown vector, AAV-sh-*Atp6i*, completely inhibited bone resorption through abolishment of extracellular acidification function of osteoclasts (Fig. 2). It also reduced the inflammatory cell infiltrate, including $CD3^+$ T cells. Our study is the first to report the use of *Atp6i*/*TIRC7* gene knockdown as a viable gene therapy strategy for oral disease.

To investigate the mechanism of the AAV-sh-*Atp6i* effect *in vivo*, we found that *Atp6i* expression was decreased (Fig. 3) and that the *Atp6i* knockdown abolished extracellular acidification and inhibited bone resorption (Fig. 4). Of interest, osteoclast numbers were also decreased in the AAV-sh-*Atp6i* treatment group, as indicated by reduced TRAP staining, and reduced expression of cathepsin K and Acp5. The expression level of macrophage marker *CD115* mRNA was also reduced in the AAV-sh-*Atp6i* treatment group, indicating fewer macrophages in the periapical lesions. Our macrophage marker (F4/80) immunohistochemistry stain confirmed that there were fewer macrophages in the periapical lesions in the AAV-sh-*Atp6i* group than in the AAV-sh-Luc-YFP group (see Fig. S2 in the supplemental material). Levels of inflammatory mediators, including IL-1a, IL-1β, IL-17,

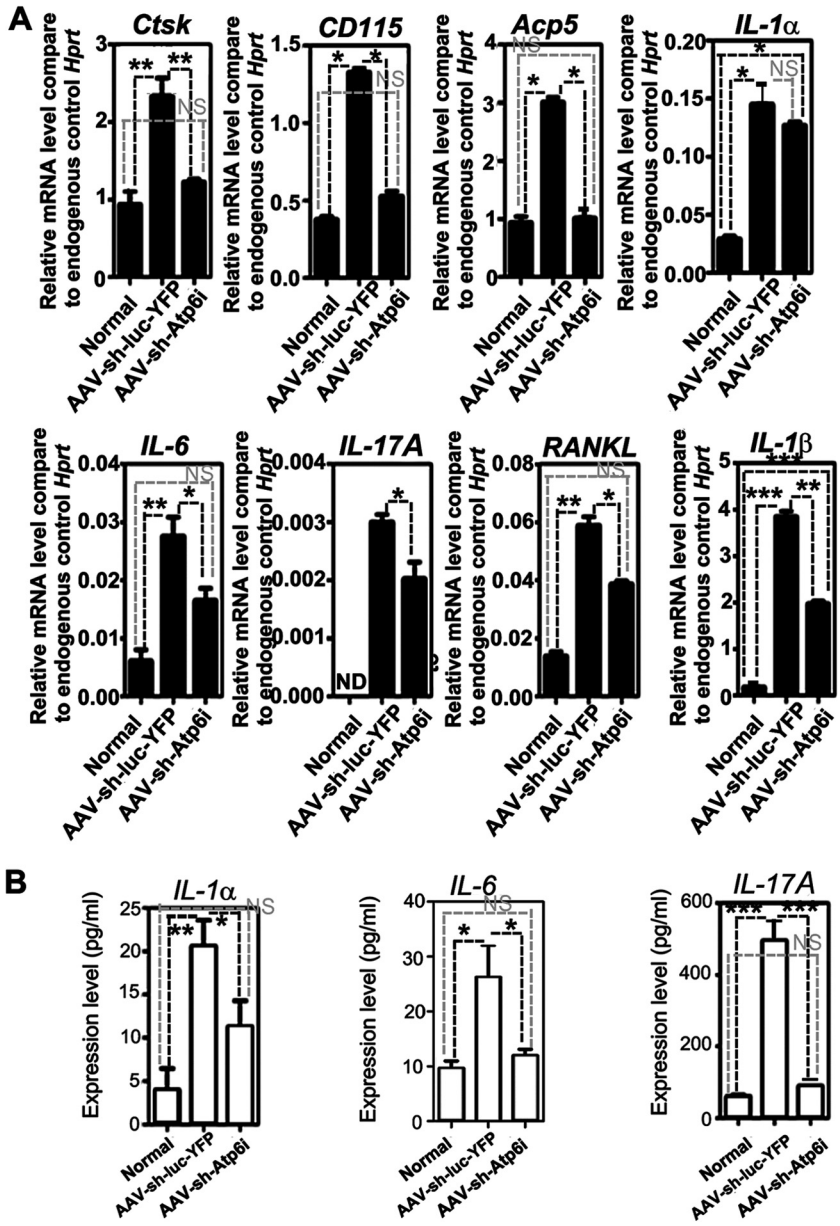

FIG 6 AAV-sh-*Atp6i* reduced the expression of osteoclast marker genes and cytokines in periapical lesions. (A) qPCR of osteoclast marker genes (i.e., cathepsin K and Acp5), genes important for osteoclast differentiation (i.e., RANKL), a gene common to macrophages and osteoclasts (i.e., CD115), and cytokines (i.e., IL-6, IL-1α, IL-1β, and IL-17α) in the periapical lesion from uninfected mice (normal) or infected mice treated with AAV-sh-Luc-YFP or with AAV-sh-*Atp6i*. *Hprt* was used as an endogenous control. (B) IL-1α, IL-6, and IL-17α levels in the periapical lesion as detected by ELISA. NS, not significant; *, $P < 0.05$; **, $P < 0.01$; ***, $P < 0.005$.

IL-6, and the osteoclast inducer RANKL, were also reduced by AAV-sh-*Atp6i* (Fig. 6). It has been reported that T and B lymphocytes are major sources of RANKL in the bone resorptive lesion of periodontitis (11), and our finding that T-cell numbers were reduced in periapical lesions in the AAV-sh-Atp6i treatment group is consistent with this observation (Fig. 5). Finally, the capacity of AAV-sh-Atp6i treatment to dramatically reduce inflammation and bone resorption in infected mice was observed 21, 28, and 42 days after infection (Fig. 5; also, see Fig. S1 in the supplemental material). Taken together, although further studies are needed, the effect of AAV-sh-Atp6i on osteoclast numbers may represent a direct effect on osteoclast differentiation but also may result indirectly from inhibition of T-cell activation and inflammation.

AAV gene therapy has been reported in models of periodontal disease, which, like periapical disease, are induced by bacterial infection. Systemic transduction with TIMP-4 was reported to reduce both adjuvant-induced arthritis and periodontitis in rats (39). Inhibition of periodontal bone loss following AAV gene transfer of mitogen-activated protein kinase phosphatase-1 (MKP-1), which dephosphorylates MAPKs and inhibits immune responses, was also reported (40). Transduction of gingival tissues with AAV/2/1-tumor necrosis factor receptor-immunoglobulin

Fc (TNFR:Fc) (41) reduced *P. gingivalis*-induced periodontal bone loss by approximately 50% in a mouse model, with parallel reductions in proinflammatory cytokines and osteoclasts (41). In the latter study, the AAV-TNFR:Fc vector was delivered three times per week for 8 weeks, compared to two injections of AAV-sh-Atp6i in the present work. The greater efficiency of Atp6i inhibition (80%) may reflect the critical importance of the proton pump for osteoclast function, given that both humans and mice with Atip61 deficiency are severely osteopetrotic (7). In addition, the simultaneous targeting of a gene critical for T-cell response induction (*TIRC7*) may have additive effects on the prevention of inflammatory bone loss.

IL-1α promotes osteoclast differentiation via the tyrosine kinase–NF-κB pathway (42), and IL-1α mRNA and protein levels were reduced in the AAV-sh-*Atp6i* group. Similarly, IL-1β levels were increased in the periapical lesion of disease model group, and were significantly reduced by AAV-sh-*Atp6i* (Fig. 6). Some studies indicate that IL-6 promotes bone resorption and periapical lesion development (43). AAV-sh-Atp6i treatment reduced IL-6 levels in the AAV-sh-Atp6i-treated group compared to IL-6 levels in the periapical lesions of the AAV-sh-Luc-YFP-treated disease model group. Th17 is a third subset of effector T helper cells that produce IL-17α (44), which may play an important role in the initiation and maintenance of proinflammatory responses and was recently found to stimulate osteoclastic resorption (45). It was recently reported that the expression of IL-17α mRNA was significantly induced in periapical lesions of wild-type mice after infection and that IL-17α, but not gamma interferon (IFN-γ) or tumor necrosis factor alpha (TNF-α), plays an important role in the formation of periapical lesions (46).

In summary, we investigated the therapeutic effect of AAV-sh-*Apt6i* that simultaneously targeted the osteoclastic gene *Atp6i* and the T-cell gene *TIRC7*. AAV-sh-*Apt6i* reduced the bone resorption by both direct inhibition of osteoclast acidification function and inflammation and thus decreased osteoclast differentiation. This suggests that a gene therapy approach may be highly effective in reducing the severity of periapical disease *in vivo*.

ACKNOWLEDGMENTS

We thank Christie Paulson and Zach Nolen for their excellent assistance with the manuscript. In addition, we thank Sergei Musatov and Sonoko Ogawa for kindly providing the AAV-H1-shRNA-Luc-YFP and AAV-H1 vectors and helpful suggestions. We appreciate the assistance of the Center for Metabolic Bone Disease at the University of Alabama at Birmingham (P30 AR046031). We are also grateful for the assistance of the Small Animal Phenotyping Core, Metabolism Core, Histomorphometry and Molecular Analyses Core, Neuroscience Image Core, and Neuroscience Molecular Detection Core Laboratory at the University of Alabama at Birmingham (P30 NS0474666).

This work was supported by NIH grants RC1-DE-020533 (Y.P.L.) and R01-AR-055307 (Y.P.L.).

We declare no competing financial interests.

REFERENCES

1. **World Health Organization.** 12 September 2012, date accessed. Oral health. World Health Organization, Geneva, Switzerland. http://www.who.int/oral_health/disease_burden/global/en/.
2. **Nair PN.** 1997. Apical periodontitis: a dynamic encounter between root canal infection and host response. Periodontol. 2000 **13**:121–148.
3. **Stashenko P.** 1990. Role of immune cytokines in the pathogenesis of periapical lesions. Endod. Dent. Traumatol. **6**:89–96.
4. **Kakehashi S, Stanley HR, Fitzgerald RJ.** 1965. The effects of surgical exposures of dental pulps in germ-free and conventional laboratory rats. Oral Surg. Oral Med. Oral Pathol. **20**:340–349.
5. **Nair PN.** 2004. Pathogenesis of apical periodontitis and the causes of endodontic failures. Crit. Rev. Oral Biol. Med. **15**:348–381.
6. **Feng S, Deng L, Chen W, Shao J, Xu G, Li YP.** 2009. Atp6v1c1 is an essential component of the osteoclast proton pump and in F-actin ring formation in osteoclasts. Biochem. J. **417**:195–203.
7. **Li YP, Chen W, Liang Y, Li E, Stashenko P.** 1999. Atp6i-deficient mice exhibit severe osteopetrosis due to loss of osteoclast-mediated extracellular acidification. Nat. Genet. **23**:447–451.
8. **Uchiyama M, Nakamichi Y, Nakamura M, Kinugawa S, Yamada H, Udagawa N, Miyazawa H.** 2009. Dental pulp and periodontal ligament cells support osteoclastic differentiation. J. Dent. Res. **88**:609–614.
9. **Yamaguchi M, Aihara N, Kojima T, Kasai K.** 2006. RANKL increase in compressed periodontal ligament cells from root resorption. J. Dent. Res. **85**:751–756.
10. **Kojima T, Yamaguchi M, Kasai K.** 2006. Substance P stimulates release of RANKL via COX-2 expression in human dental pulp cells. Inflamm. Res. **55**:78–84.
11. **Kawai T, Matsuyama T, Hosokawa Y, Makihira S, Seki M, Karimbux NY, Goncalves RB, Valverde P, Dibart S, Li YP, Miranda LA, Ernst CW, Izumi Y, Taubman MA.** 2006. B and T lymphocytes are the primary sources of RANKL in the bone resorptive lesion of periodontal disease. Am. J. Pathol. **169**:987–998.
12. **Lin X, Han X, Kawai T, Taubman MA.** 2011. Antibody to receptor activator of NF-kappaB ligand ameliorates T cell-mediated periodontal bone resorption. Infect. Immun. **79**:911–917.
13. **Heinemann T, Bulwin GC, Randall J, Schnieders B, Sandhoff K, Volk HD, Milford E, Gullans SR, Utku N.** 1999. Genomic organization of the gene coding for TIRC7, a novel membrane protein essential for T cell activation. Genomics **57**:398–406.
14. **Utku N, Boerner A, Tomschegg A, Bennai-Sanfourche F, Bulwin GC, Heinemann T, Loehler J, Blumberg RS, Volk HD.** 2004. TIRC7 deficiency causes in vitro and in vivo augmentation of T and B cell activation and cytokine response. J. Immunol. **173**:2342–2352.
15. **Utku N, Heinemann T, Winter M, Bulwin CG, Schlawinsky M, Fraser P, Nieuwenhuis EE, Volk HD, Blumberg RS.** 2006. Antibody targeting of TIRC7 results in significant therapeutic effects on collagen-induced arthritis in mice. Clin. Exp. Immunol. **144**:142–151.
16. **Kaplitt MG, Feigin A, Tang C, Fitzsimons HL, Mattis P, Lawlor PA, Bland RJ, Young D, Strybing K, Eidelberg D, During MJ.** 2007. Safety and tolerability of gene therapy with an adeno-associated virus (AAV) borne GAD gene for Parkinson's disease: an open label, phase I trial. Lancet **369**:2097–2105.
17. **Carter BJ.** 2005. Adeno-associated virus vectors in clinical trials. Hum. Gene Ther. **16**:541–550.
18. **Gasmi M, Herzog CD, Brandon EP, Cunningham JJ, Ramirez GA, Ketchum ET, Bartus RT.** 2007. Striatal delivery of neurturin by CERE-120, an AAV2 vector for the treatment of dopaminergic neuron degeneration in Parkinson's disease. Mol. Ther. **15**:62–68.
19. **Musatov S, Chen W, Pfaff DW, Kaplitt MG, Ogawa S.** 2006. RNAi-mediated silencing of estrogen receptor a in the ventromedial nucleus of hypothalamus abolishes female sexual behaviors. Proc. Natl. Acad. Sci. U. S. A. **103**:10456–10460.
20. **Sasaki H, Suzuki N, Kent R, Jr, Kawashima N, Takeda J, Stashenko P.** 2008. T cell response mediated by myeloid cell-derived IL-12 is responsible for Porphyromonas gingivalis-induced periodontitis in IL-10-deficient mice. J. Immunol. **180**:6193–6198.
21. **Wilensky A, Polak D, Awawdi S, Halabi A, Shapira L, Houri-Haddad Y.** 2009. Strain-dependent activation of the mouse immune response is correlated with Porphyromonas gingivalis-induced experimental periodontitis. J. Clin. Periodontol. **36**:915–921.
22. **Yang S, Chen W, Stashenko P, Li YP.** 2007. Specificity of RGS10A as a key component in the RANKL signaling mechanism for osteoclast differentiation. J. Cell Sci. **120**:3362–3371.
23. **Yang S, Li YP.** 2007. RGS10-null mutation impairs osteoclast differentiation resulting from the loss of [Ca2+]i oscillation regulation. Genes Dev. **21**:1803–1816.
24. **Kelly KA, Tanaka S, Baron R, Gimble JM.** 1998. Murine bone marrow stromally derived BMS2 adipocytes support differentiation and function of osteoclast-like cells in vitro. Endocrinology **139**:2092–2101.
25. **Kurland JI, Kincade PW, Moore MA.** 1977. Regulation of B-lymphocyte

clonal proliferation by stimulatory and inhibitory macrophage-derived factors. J. Exp. Med. **146**:1420–1435.
26. **Alexander B, Warner-Schmidt J, Eriksson T, Tamminga C, Arango-Lievano M, Ghose S, Vernov M, Stavarache M, Musatov S, Flajolet M, Svenningsson P, Greengard P, Kaplitt MG.** 2010. Reversal of depressed behaviors in mice by p11 gene therapy in the nucleus accumbens. Sci. Transl. Med. 2:54ra76.
27. **Hommel JD, Sears RM, Georgescu D, Simmons DL, DiLeone RJ.** 2003. Local gene knockdown in the brain using viral-mediated RNA interference. Nat. Med. **9**:1539–1544.
28. **Tomar RS, Matta H, Chaudhary PM.** 2003. Use of adeno-associated viral vector for delivery of small interfering RNA. Oncogene **22**:5712–5715.
29. **Kawashima N, Niederman R, Hynes RO, Ullmann-Cullere M, Stashenko P.** 1999. Infection-stimulated infraosseus inflammation and bone destruction is increased in P-/E-selectin knockout mice. Immunology **97**: 117–123.
30. **Sasaki H, Hou L, Belani A, Wang CY, Uchiyama T, Muller R, Stashenko P.** 2000. IL-10, but not IL-4, suppresses infection-stimulated bone resorption in vivo. J. Immunol. **165**:3626–3630.
31. **Balto K, Muller R, Carrington DC, Dobeck J, Stashenko P.** 2000. Quantification of periapical bone destruction in mice by micro-computed tomography. J. Dent. Res. **79**:35–40.
32. **von Stechow, D, Balto K, Stashenko P, Muller R.** 2003. Three-dimensional quantitation of periradicular bone destruction by micro-computed tomography. J. Endod. **29**:252–256.
33. **Balto K, White R, Mueller R, Stashenko P.** 2002. A mouse model of inflammatory root resorption induced by pulpal infection. Oral Surg. Oral Med. Oral Pathol. Oral Radiol. Endod. **93**:461–468.
34. **Yang S, Wei D, Wang D, Phimphilai M, Krebsbach PH, Franceschi RT.** 2003. In vitro and in vivo synergistic interactions between the Runx2/Cbfa1 transcription factor and bone morphogenetic protein-2 in stimulating osteoblast differentiation. J. Bone Miner. Res. **18**:705–715.
35. **Jules J, Shi Z, Liu J, Xu D, Wang S, Feng X.** 2010. Receptor activator of NF-κB (RANK) cytoplasmic IVVY535-538 motif plays an essential role in tumor necrosis factor α (TNF)-mediated osteoclastogenesis. J. Biol. Chem. **285**:37427–37435.
36. **Allaire JM, Darsigny M, Marcoux SS, Roy SA, Schmouth JF, Umans L, Zwijsen A, Boudreau F, Perreault N.** 2011. Loss of Smad5 leads to the disassembly of the apical junctional complex and increased susceptibility to experimental colitis. Am. J. Physiol. Gastrointest. Liver Physiol. **300**: G586–G597.
37. **Nijenhuis T, van der Eerden BC, Hoenderop JG, Weinans H, van Leeuwen JP, Bindels RJ.** 2008. Bone resorption inhibitor alendronate normalizes the reduced bone thickness of TRPV5(-/-) mice. J. Bone Miner. Res. **23**:1815–1824.
38. **Sasaki H, Okamatsu Y, Kawai T, Kent R, Taubman M, Stashenko P.** 2004. The interleukin-10 knockout mouse is highly susceptible to Porphyromonas gingivalis-induced alveolar bone loss. J. Periodontal Res. **39**: 432–441.
39. **Ramamurthy NS, Greenwald RA, Celiker MY, Shi EY.** 2005. Experimental arthritis in rats induces biomarkers of periodontitis which are ameliorated by gene therapy with tissue inhibitor of matrix metalloproteinases. J. Periodontol. **76**:229–233.
40. **Yu H, Li Q, Herbert B, Zinna R, Martin K, Junior CR, Kirkwood KL.** 2011. Anti-inflammatory effect of MAPK phosphatase-1 local gene transfer in inflammatory bone loss. Gene Ther. **18**:344–353.
41. **Cirelli JA, Park CH, MacKool K, Taba M, Jr, Lustig KH, Burstein H, Giannobile WV.** 2009. AAV2/1-TNFR:Fc gene delivery prevents periodontal disease progression. Gene Ther. **16**:426–436.
42. **Kamolmatyakul S, Chen W, Yang S, Abe Y, Moroi R, Ashique AM, Li YP.** 2004. IL-1alpha stimulates cathepsin K expression in osteoclasts via the tyrosine kinase-NF-kappaB pathway. J. Dent. Res. **83**:791–796.
43. **Lin SK, Kok SH, Kuo MY, Wang TJ, Wang JT, Yeh FT, Hsiao M, Lan WH, Hong CY.** 2002. Sequential expressions of MMP-1, TIMP-1, IL-6, and COX-2 genes in induced periapical lesions in rats. Eur. J. Oral Sci. **110**:246–253.
44. **Korn T, Bettelli E, Oukka M, Kuchroo VK.** 2009. IL-17 and Th17 Cells. Annu. Rev. Immunol. **27**:485–517.
45. **Sato K, Suematsu A, Okamoto K, Yamaguchi A, Morishita Y, Kadono Y, Tanaka S, Kodama T, Akira S, Iwakura Y, Cua DJ, Takayanagi H.** 2006. Th17 functions as an osteoclastogenic helper T cell subset that links T cell activation and bone destruction. J. Exp. Med. **203**:2673–2682.
46. **Oseko F, Yamamoto T, Akamatsu Y, Kanamura N, Iwakura Y, Imanishi J, Kita M.** 2009. IL-17 is involved in bone resorption in mouse periapical lesions. Microbiol. Immunol. **53**:287–294.